Deformation of the Zhangjiazhuang high-speed railway tunnel: an analysis of causal mechanisms using geomorphological surveys and D-InSAR monitoring

Deformation of the Zhangjiazhuang high-speed railway tunnel: an analysis of causal mechanisms using geomorphological surveys and D-InSAR monitoring

MENG Xing-min[1,2,3] https://orcid.org/0000-0003-3102-6193; e-mail: xmmeng@lzu.edu.cn
QI Tian-jun[2,3*] https://orcid.org/0000-0003-0794-2570; e-mail: qitj16@lzu.edu.cn
ZHAO Yan[1,3] https://orcid.org/0000-0003-1180-8868; e-mail:zhaoy16@lzu.edu.cn
DIJKSTRA Tom[4] https://orcid.org/0000-0002-9851-6499; e-mail: T.A.Dijkstra@lboro.ac.uk
SHI Wei[2,3] https://orcid.org/0000-0001-6096-0896; e-mail: shiw19@lzu.edu.cn
LUO Yin-fei[5] https://orcid.org/0000-0001-8293-5990; e-mail: 478967346@qq.com
WU Yuan-zhao[5] https://orcid.org/0000-0002-6466-6798; e-mail: 460504937@qq.com
SU Xiao-jun[2,3] https://orcid.org/0000-0003-4895-9782; e-mail: suxj19@lzu.edu.cn
ZHAO Fu-meng[2,3] https://orcid.org/0000-0002-8068-1584; e-mail: zhaofm13@lzu.edu.cn
MA Jin-hui[2,3] https://orcid.org/0000-0003-2656-9126; e-mail: majh@lzu.edu.cn
ZHANG Yi[1,3] https://orcid.org/0000-0001-7105-9497; e-mail: zhangyigeo@lzu.edu.cn
CHEN Guan[1,3] https://orcid.org/0000-0001-8834-039X; e-mail: gchen@lzu.edu.cn
YUE Dong-xia[2,3] https://orcid.org/0000-0002-9007-2117; e-mail: dxyue@lzu.edu.cn
ZHANG Mao-sheng[6] https://orcid.org/0000-0001-9150-8851; e-mail: xazms@126.com

*Corresponding author
[1] School of Earth Sciences, Lanzhou University, Lanzhou 730000, China
[2] College of Earth and Environmental Sciences, MOE Key Laboratory of Western China's Environmental Systems, Lanzhou University, Lanzhou 730000, China
[3] Gansu Tech Innovation Centre for Environmental Geology and Geohazard Prevention, Lanzhou 730000, China
[4] School of Architecture, Building and Civil Engineering, Loughborough University, Loughborough, LE11 3TU, UK
[5] Key Laboratory of Qinghai Environmental Geological Survey, Xining 810007, China
[6] Xi'an Centre of China Geological Survey, Xi'an 710054, China

Abstract:

On 18 January 2016, the Zhangjiazhuang high-speed railway tunnel in Ledu, Qinghai Province, China, underwent serious deformation and structural damage. A crack formed at the top of the tunnel and the concrete on the crown peeled off. As a result, the tunnel could not be operated for three months. In order to determine the types and spatial distribution of the landslides in the region and the surface deformation characteristics associated with the tunnel deformation, we used field geological and geomorphological surveys, unmanned aerial vehicle image interpretation and differential interferometric synthetic aperture radar (D-InSAR) surface deformation monitoring. Nine ancient and old landslides were identified and analysed in the study area. Surface deformation monitoring and investigation of buildings in several villages on the slope front showed that the tunnel deformation was not related to deep-seated gravitational slope deformation. However, surface deformation monitoring revealed an active NEE–SWW fault in the area intersecting the tunnel at the location of the tunnel rupture. This constitutes a plausible mechanism for the deformation of the tunnel. Our study highlights the need for detailed engineering geomorphological investigations to better predict the occurrence of tunnel deformation events in the future.

Keywords: Gaojiawan; Landslide group; Zhangjiazhuang tunnel; Deformation; Fault activity; Irrigation infiltration

1 Introduction

With the rapid development of the global economy and the intensification of human activities in recent decades, the density of transport networks has increased rapidly. Tunnels play an increasingly important role in transport network construction in mountainous areas (He and Wang 2013). However, these regions are also subject to geological and slope processes, such as tectonic activity, deep-seated gravitational slope deformation, groundwater seepage, and landslide reactivation that can result in tunnel deformation and threaten transport safety (Obradovic 1990; Konagai et al. 2005; Fernandez and Moon 2010; Wang et al. 2011; Farhadian et al. 2012; Causse et al. 2015). Although the rapid development of materials science, engineering, geophysics, remote sensing, and other disciplines provides strong support for engineering construction, tunnel safety is still not fully guaranteed, particularly when local conditions are poorly understood or not fully investigated.

The interplay between landslides and tunnels is extremely complex (Mao and Zhou 2002; Bandini et al. 2015; Vassallo et al. 2019). Spatially, tunnels can cross a landslide or sliding surface, they can be positioned below a slip surface, or a new landslide can be induced by tunnel excavation (Wu et al. 2012). This spatial relationship controls the nature and scale of tunnel deformation (Wu and Pai 2020). Many structural models have been proposed to determine the interactions between tunnels and landslides as these spatial relationships lead to significant differences in stress characteristics and deformation (Ma and Wu 2016). Zhang et al. (2017) developed a 'slip line' theory which included obtaining the range of disturbance caused by tunnel excavation and determining the minimum safe distance between the tunnel vault and slip zone. Gattinoni (2019) studied the influence of deep-seated gravitational slope deformation on tunnels, and Zhang et al. (2015) studied the mechanical conditions of landslides induced by tunnel excavation. Various research methods are being used to analyse the relationship between landslides and tunnels, including detailed geological and geomorphic investigation, three-dimensional numerical simulation, surface deformation monitoring based on InSAR technology, and GPS/GNSS monitoring (Tang et al. 2013; Singh et al. 2014; Troncone et al. 2014; Barla et al. 2015; Nikadat et al. 2015; Zhang et al. 2015; Komu et al. 2020). InSAR technology, a high-precision remote sensing monitoring method provides capabilities for monitoring surface movement (Flessandro et al. 2001; Zhang et al. 2016); however, surface movement monitoring alone may not be sufficient to explain the underlying mechanism of slope deformation. Traditional engineering geomorphological investigations, coupled with invasive investigations from boreholes, remain important, particularly for the investigation of the spatial distribution and slip surface morphology of large landslides that could potentially intersect a tunnel. In addition to landslides, geological structures (joint sets, faults, bedding, etc.) are also important factors that require careful examination before tunnel construction commences. However, this is not always easy, as is demonstrated by the frequent cases of tunnel deformation caused by joint fabric, fault activity, and the occurrence of a weak surface within the stratum (Li and Chen 1999; Zhang et al. 2013).

The Zhangjiazhuang tunnel is located in the Gansu to Qinghai section of the East-West Highspeed railway in China. This section is the core component of the transport network in Western China. The tunnel construction commenced in 2010 and was completed in early 2012. On 18 January 2016, substantial tunnel deformation occurred, with a crack (from DK120+300 to DK120+930) developing along the top of the tunnel. This resulted in numerous concrete blocks of the tunnel lining becoming dislodged and falling onto the rail tracks. It was reported that the largest of these concrete blocks contained steel reinforcements with diameters of several tens of centimetres. Fortunately, due to the timely discovery of the damage to the tunnel and track, emergency measures were imposed and casualties were avoided. However, the closure of the tunnel resulted in significant economic losses and inconvenience. Some degree of precedent was noted: in October 2011, local residents discovered a crack extending for ~1 km along the main scarp of the old landslide, which was located above the

tunnel. In addition, the walls of the factory at the front of the slope had undergone varying degrees of deformation, which preceded the tunnel deformation.

In 2017, a project was implemented to conduct a comprehensive survey of the area of the Zhangjiazhuang tunnel disaster. Although it was established that many old landslides had developed in the area, the influence of long-term runoff, erosion, afforestation and other factors obscured the morphological characteristics of these old landslides, making it more difficult to identify their features and outlines. It was therefore important to carry out a detailed investigation and to determine the landslide distribution pattern at the site.

The following specific research questions were addressed in the study: (i) What caused the deformation of the tunnel and the wall along the toe of the slope in the north-eastern part of the study area? (ii) What caused the reactivation of major landslides in the area? (iii) Is there a relationship between the reactivation of landslide and the construction and operation of the tunnel?

2 Regional Setting

2.1 Study area

The study area is located in the approximate geometric centre of the land territory of China (36°24′42″–36°27′24″N, 102°30′10″–102°33′06″E) (Fig. 1). To the north of the area there is the wide, flat valley of the Huangshui River, which is a major tributary of the Yellow River. In addition, several important routeways connecting east and west China, such as the Beijing-Lhasa Highway, the G109 national Highway and the Qinghai-Tibet Railway, transit the area. Four villages are located in the northern part of the study area. One of these, Gaojiawan is located at the front of the slope; it comprises 167 households with a total population of 650. Reactivation of the landslide therefore poses a risk to the lives, property and well-being of the inhabitants of Gaojiawan village and the neighboring areas.

The study area is located in the eastern part of the Qinghai-Tibet Plateau and on the western edge of the Loess Plateau. It has a temperate semi-arid climate. According to data from meteorological stations in the Ledu region, the annual average temperature in the region is 7.3°C; an extreme maximum temperature of 38.4°C was recorded in July of 2000, and an extreme minimum temperature of -21.7°C in December 1975. The annual average precipitation is 329.6 mm, with a maximum of 484 mm recorded in 2018.

2.2 Topography

The elevation of the study area ranges from 1,903–2,466 m a.s.l. (Fig. 1); the highest point is located in the southern part of the study area and the lowest point is in the valley of the Huangshui river. Thick loess covers the Paleogene mudstone and sandy-mudstone in the area and erosional processed during the late Pleistocene and Holocene have left a significant imprint on the geomorphology. One of the deepest gullies has developed in very thick loess (~144 m maximum thickness), exposing the underlying bedrock. The formation of sinkholes and gullies appears to be affected by sub-vertical joints in the loess. These joints affect the location pattern of sinkholes resulting in a bead-like pattern (Fig. 2). Landslide features also appear to affect the location of these sinkholes, with many occurring along scarps and on landslide bodies (Derbyshire et al. 2000). These sinkholes are of varying sizes, with diameters ranging from tens of centimetres to several meters and with depths up to several tens of meters. Following the deformation of the tunnel, these sinkholes, which are very significant for the development of loess landslides, have been sealed (Fig. 2). Although the slope mass is affected by weathering, several landslide features are preserved; in particular, the main scarp of the dominant landslide is clearly visible. During the Quaternary, the area was influenced by the uplift of the Qinghai-Tibet Plateau, resulting in the development of terraces I–V of the Huangshui River in the Gaojiawan area. This study focuses on the investigation of the fourth and fifth terraces (Fig. 2), which are relevant to the identification of landslides.

2.3 Stratigraphy and Lithology

The stratigraphy of the study area consists mainly of Quaternary loose loess and Paleogene mudstone and sandy-mudstone (Figure 3). According to the results of previous studies (Song 2006), field investigations and drilling data, the strata in the study area comprise the following, from bottom to top: (i) The Paleocene Qijiachuan Formation, the lithology of which is brown-red conglomerate with intercalated sandstone (Figure 4a and 4b). (ii) The Eocene Honggou Formation, which is composed of three litho-stratigraphic units. The lower unit consists of brown-red mudstone; the middle unit consists of grey-green banded mudstone and brown-red mudstone interbedded with brick-red mudstone; and the upper unit consists of grey-green gypsum intercalated with glauberite and lime-yellow marl. Based on the method introduced by Hoek and Brown (1997) to evaluate rock mass quality, the Geological Strength Index (GSI) of these layers has the range of 70–80. The dominant strike of the units is 130°–175° and the dip angle is 3°–7°. (iii) Quaternary loess. According to borehole data, the loess in the region is up to 144 m thick. Zhou et al. (2020) determined that the friction angle and cohesion of loess and mudstone, based on a consolidated quick shear test, are 26°, 22 KPa and 35°, 28 KPa, respectively. The terraces of the Huangshui River are distributed in the northern part of the study area; the thickness of the gravel layers of terraces is up to 19 m (Fig. 4c).

2.4 Geological structure

The study area is located in Xining Basin in the north-eastern part of the Qinghai-Tibet Plateau (Fig. 5). The Xining Basin was an extensional basin in the Early Cenozoic, but changed into a compressive basin during the Late Cenozoic. The formation and deformation of the Xining Basin are direct responses to the India-Eurasia collision and the growth of the Qinghai-Tibet Plateau (Zhang et al. 2016). The northern margin of the basin is controlled by the Daban Mountain fault, and the southern margin is restricted by the Lajishan fault. The basement is composed of the pre-Sinian system, above which Triassic strata are distributed, and it is composed of coal and clastic sediments, with a thickness of 435 m. The upper and lower Cretaceous series have high rock mass quality, comprising fluvial and lacustrine red sandstone and conglomerate; the thickness is 163 m and there is an angular unconformity between the upper and lower series. Under the influence of the Qinghai-Tibet Plateau, the strata of the interior of the basin were subjected to NNE compression; N–S trending structures are relatively well developed and the folds are open and gentle. There are two groups of joints developed in the region; the strike of one group has the range of 35°–70°, and the other the range of 160°–170°. The principal stress direction indicated by the rose diagram of the joint is NNE (Fig. 2). Neotectonic movements have significantly affected the area: in a roadside profile, we observed that a Pleistocene paleosol layer with a thickness of 0.7 m was fractured by normal faulting, to a distance of 1.3 m, with a strike of 110°, and a fault has fractured the sandstone layers sandwiched within the mudstone (Figs. 6a and 6b).

3 Methods

Landscape evolution affected by neotectonic movement, surface erosion and human activity have resulted in the formation of a complex landslide in the study area. To collect evidence and to determine the relationship between the tunnel deformation and landslides, we conducted engineering geological and geomorphological surveys, drilled a series of boreholes, and carried out surface topography surveys using small unmanned aerial vehicle (UAV) images to reconstruct the spatial distribution of the landslide group. In recent years, the rapid development of small UAVs, space-borne radar surveying, 3D scanning, electrical resistivity, and other technologies has provided strong support for the investigation of landforms that potentially pose a significant risk to society (Syahmi et al. 2011; Ma et al. 2014; Ma et al. 2015; Liu et al. 2015; Zeng et al. 2016; Qi et al. 2021). In the early stages of the investigations, we aimed to use UAV images to precisely interpret the surface elements within the scope of the tunnel excavation, including sinkholes, sealed sinkholes, irrigation areas, landslide boundaries, and surface cracks. With the rapid development of remote sensing technology, traditional landform survey methods for the investigation of a (potential) geohazard are

gradually becoming marginalised. Nevertheless, traditional field surveys still have advantages, particularly when, as in this case, a forensic analysis of landforms is required.

Considering the dense landslide group on the slope above the Zhangjiazhuang tunnel, there is a complex overlapping relationship between different landslides, which makes it difficult to accurately determine landslide boundaries using remote sensing images. Due to the weak cementation of loess, the morphological characteristics of most landslides are seriously degraded because of long-term rainfall induced erosion. This study aimed to reconstruct the spatial distribution of the old landslide group by combining a 3m-resolution digital elevation model (DEM), UAV images, engineering geomorphological surveys, and borehole observations. For the engineering geomorphological investigation, handheld GPS and laser rangefinders were used to determine the positions of landslide boundaries, the length and position of cracks, and the dimensions of the landslide complex.

The D-InSAR technique can capture the (slow) ground deformation caused by faults or landslides (Ye et al. 2004; Casu et al. 2006). Two Sentinel-1A IW (Interferometric Wide-swath) images with a resolution of 14 m ×4 m in the azimuth and range directions, obtained on 20 December 2015 and 6 February 2016 in an ascending orbit of 128, were applied to monitor deformation in the study area. In the InSAR monitoring processing, a 5:1 ratio in the range and azimuth directions was used to resample the resolution of the images for the generation of differential interferograms. The images were also corrected to topographic effects using the 3m– resolution DEM. The Goldstein filter and minimum cost flow (MCF) with a coherence threshold of 0.35 were used in the D-InSAR process of filtering and phase unwrapping (Aimaiti et al. 1998; Costantini 1998; Goldstein and Werner 1998; Rehman et al. 2020).

4 Tunnel Damage Distribution and Characteristics of Ancient Landslides

4.1 Tunnel characteristics and damage

Construction of the Zhangjiazhuang tunnel began in early 2010 and was completed in the first half of 2012; full operation began in 2014. The tunnel is a single bore, double track, high-speed railway tunnel with a total length of 3769 m (DK118+595- DK122+364) and a longitudinal slope of 3.5‰. The shotcrete anchor method was adopted in the construction of the project. The rock mass rating (Bieniawski 1973) was used to grade the surrounding rock along the tunnel as IV to V. The tunnel section, surrounding rock type, and corresponding parameters refer to the study of Zhou et al. (2020). On 18 January 2016, the top and side walls of the DK120+300- DK120+930 section of Zhangjiazhuang tunnel were seriously deformed and a large number of 5–20 cm concrete blocks peeled off from the top of the tunnel. The deformation of the tunnel produced a longitudinal crack with a maximum width of 20 mm and a series of transverse cracks with an average spacing of 8 m and width varying from 1 to 10 mm (Zhou et al. 2020). This emergency resulted in the closure or the railway which is an important transport route connecting Central and Western China.

4.2 Distribution and characteristics of the landslide group

Loess landslides are mainly controlled by rainfall, river erosion and earthquakes (Dijkstra et al. 1994; Zhang and Liu 2010; Peng et al. 2015). These landslides are characterized by relatively low trigger thresholds and intermittent deformation behaviour. As a consequence, features of previous phases of activity are rarely well preserved. The geomorphological characteristics of the landslides in the study area have been seriously degraded through long-term surface erosion, and only a few features have been preserved. Field investigations and the interpretation of aerial photographs enabled the mapping of landslide features and associated phenomena, such as sinkholes and gullies, in order to determine the spatial distribution of nine landslides (designated L1–L9; Fig. 7). The landslides have different-shaped slip surfaces and volumes, and they overlap one another. The largest landslide (L1) of the Gaojiawan landslide group is situated in the western section of the Zhangjiazhuang tunnel (Fig. 7). It is a large landslide characterised by a rotational slip surface at the head that transforms into a more or less planar slip surface towards the toe. This is a typical feature of many large landslides where the slip surfaces are positioned mainly in loess or (partly) along a loess-bedrock interface (Derbyshire

et al. 2000). Because of its large size and distinctive characteristics, the main landslide features are relatively well preserved. The main head scarp (Fig. 8a) is clearly visible; its elevation ranges from 2,365 to 2,410 m a.s.l., the relative height difference is 40– 50 m a.s.l. , and the average slope is 45°. At the head of the landslide there are large areas of depressions with numerous sinkholes (Fig. 2). In addition, examination of one of the boreholes revealed a slicken-sided surface (Fig. 9e) located at the interface of the loess and mudstone. The western margin of this landslide is expressed as a shallow gully, within which numerous sinkholes are developed. It is likely that these sinkholes are formed where lateral shear planes along the margin of the landslide have resulted in disturbance of the loess fabric. The eastern edge of the landslide is a deep gully formed by precipitation driven runoff and erosion. Ongoing erosion has resulted in the formation of loess collapse features and landslides are common along both sides of the gully. In places, the lower bedrock is exposed and the upper and lower binary structure of the slope can be clearly seen. This enabled the determination of the characteristic dip and strike of the bedrock underlying the loess. Field observations revealed no further evidence of slope deformation of the bedrock. Together with the slicken-sided surfaces observed in the borehole, this suggests that the landslide is a loess-mudstone interface landslide, the most common type of landslide developed in this part of the Loess Plateau (Fig. 10b). The striated surfaces indicate a slide direction of the landslide of 31° (Fig. 9d). This large-scale landslide did not impact the river terrace at the front of the slope (Fig. 2). Therefore, it is inferred that the exit location of the shear plane of the landslide is not at the foot of the slope, rather, it is within a trench along the back edge of the fourth terrace (Fig. 2). However, it has not been possible to locate this exit shear surface due to local deformation of the landslide mass in a broad compression zone. On the eastern side of the main landslide, the slope is unstable due to gully incision.

After formation of the first main landslide (L1) two further landslides (L2 and L3) developed in the eastern flank of L1 (Fig. 7), most likely following progressive incision of the main gully. This is supported by a sliding direction of ~70° (Fig. 9f). A stratigraphic sequence on the eastern side of the gully in the front of the L2 landslide showed a succession of mudstone-loess-mudstone-loess (Fig. 11a). The age of the mudstone in the study area is Paleogene, and the loess is Quaternary. There is no inversion of strata in this area, and therefore it is inferred that this sequence is due to the mudstone of the lower part of the L1 landslide overlying the loess on the east side of the gully when the L2 landslide occurred. In addition, a local survey identified groundwater seepage at the foot of the slope of the two landslides (L2 and L3) and this is likely to affect local slope stability (Fig. 11b). There are also two secondary landslides, L4 and L5, in front of L1, with a formation age that is probably the same as that of L1. In addition, we found that L5 had a distinct scarp and landslide margin depression (Fig. 11c), where there are numerous caves with a relatively small diameter but greater depth. The other two large-scale landslides, L7 and L8, are located on the east side of the study area. The main scarp of the landslide is relatively straight (Fig. 11d), with an elevation range of 2,176–2,307 m a.s.l., a relative height difference of 131 m, and an average slope angle of 40°. A large-scale bedrock landslide, L7, was developed along the toe of this landslide (Fig. 10c), and crown cracks (Fig. 11e) were developed at the lack edge of the slope scarp. During the investigations following the deformation of the tunnel, a series of shear-related features (squeezing and arching phenomena) were observed in the factory wall at the front edge of the tunnel (Fig. 12). However, it was not possible to establish an approximate time of formation of these features. Further, detailed investigation of the surrounding buildings in the village showed that, except for one example of the front edge of the L9 landslide, these features are only developed at the foot of the L8 landslide (see Fig. 7 for the location of these landslides). The deformation characteristics of the two sides of the factory wall are different. The degree of deformation of the west wall is relatively small and includes similar types of feature spaced at increasing intervals from north to south (32 m, 56.4 m, and 67 m). The east wall also has four distinct deformations, but the one near the north side is more pronounced than the other three. This suggests that the east wall has experienced greater compression and that the overall direction is from south to north at the foot of the L8 landslide slope.

4.3 Surface deformation monitoring based on D-InSAR technology

To better understand whether surface deformation coincided with tunnel deformation, we analysed thesurface deformation for the area from 20December 2015 to 6 February 2016, using D-InSAR analysis. The results show that there is no overall deformation on the slope during this period (Fig. 13) —that is, it was not possible to observe ground surface movement indicative of deep-seated gravitational slope deformation. The main surface movements are concentrated in the L2 and L3 landslides units on the western side of the main gully, which is consistent with the simulation results obtained by Zhou et al. (2020). However, due to the position in the landscape, this type of loess-mudstone landslide activity cannot pose a threat to the tunnel (Fig. 10d). Second, the front of the slope is partially uplifted, which may be related to the reactivation of secondary landslides (L8, L9). Our field investigation found that a large area has been excavated in recent years (Fig. 14a). Concurrently, due to the growing demand for cash crops, irrigation has been carried out throughout the year (Fig. 14b). The reactivation of the secondary landslide at the front may be closely related to human activities. As the position of the factory wall deformation is close to the location of the uplift, it appears that there is a relationship between the two. The deformation results on the western side of the gully show that there is a NE–SW–striking fault in this part. The extension of the fault in the southwest direction is consistent with the position of the tunnel deformation. Therefore, we speculate that tunnel deformation occurred as the result of fault activity.

5 Discussion

5.1 Spatial relationship between the landslide group and the tunnel

The main purpose of this study was to reconstruct the spatial distribution of landslides in the Gaojiawan area by combining the investigation and analysis of the geomorphological characteristics and interpretation of UAV images. The landslide types and the spatial relationship between the landslides and the tunnel are inferred, based on reconstructed slip surfaces from surface exposures and borehole information (Fig. 10). Nine landslides were identified on the slope complex in which the Zhangjiazhuang tunnel is located. According to the geomorphological characteristics and the evolution process of the surface, we infer that the formation of these old landslides is mainly affected by three factors. First, lateral erosion of the Huangshui River constitutes the main process for determining the formation of several landslides along the slope front. Second, the formation of erosion gullies in the centre of the slope results in the development of the L2, L3, and L6 landslides. Third, the high permeability of loess, coupled with the development of vertical joints, result in dense networks of sinkholes in the study area that, in turn, provide dominant infiltration conduits for rapid infiltration of rainfall and irrigation water (Fig. 10). By contrast, the underlying mudstone acts as an aquiclude and water can thus accumulate along the loess-mudstone interface where it facilitates the formation of slip surfaces. Most landslides in the study area have slip surfaces along the loessmudstone interface and both field observations and borehole records support this (Fig. 10b, 10c). Further evidence was obtained from bedrock exposures in the gullies that cut deep into the bedrock (Fig. 2). Comparison of these exposures with those outside the study area showed that the mudstone bedrock is not affected by large-scale landslides and that there is no evidence for slip surfaces located below the loessmudstone interface (Fig. 2). The entire Zhangjiazhuang tunnel is excavated within mudstone, with the top of the tunnel at least some 100 m below the loess-bedrock interface (Fig. 10d). Therefore, it can be concluded that any deformation or reactivation of the loess landslides will not affect the tunnel.

5.2 Analysis of the cause of tunnel deformation

Tunnel deformation and fracturing are generally complex engineering geology/geomorphology problems. Fault zone weakening, intersecting joint sets, seismic activity, landslides, and groundwater convergence are common causes of tunnel deformation and failure (Hoek and Marinos 2000; Konagai et al. 2005; Gattinoni et al. 2019). Considering that tunnel deformation and failure often have unpredictable consequences, research on the causes and prevention of tunnel deformation and failure has attracted much attention. For the causes of the deformation of the Zhangjiazhuang tunnel

several potential hypotheses were postulated. At first, we assumed that the deformation is the result of deepseated gravitational slope deformation. Tian et al. (2019) conducted high-density electrical resistivity, ground penetrating radar, and soil radon measurements in the front of the L8 landslide. The results indicated that the tunnel deformation is related to a deep-seated potential sliding deformation. Zhou et al. (2020) considered that tunnel deformation was related to the reactivation of the L3 landslide on the west side of the gully, and the location of the landslide was consistent with the location of the tunnel failure. However, these observations have significant limitations. In the former, the detection of a landslide was limited to the front edge, and no sign of deep gravitational deformation was detected. In addition, according to our survey results, the paved highway at the front of the slope was not damaged, and the deformation of the factory wall at the front edge of the slope shows that it was the result of local displacements, rather than deep-seated gravitational slope deformation. Although the simulation results agree with the landslide fracture location, the simulations carried out in the latter study did not consider the material conditions of the stratum interface, and the influence of the old landslide. Both studies lacked systematic geomorphological investigations and they did not perform a detailed analysis of the causes and spatial distribution of the old and ancient landslides. Investigation of the geological and geomorphological characteristics of the Gaojiawan coupled with the interpretation of UAV images have provided a better understanding of the spatial distribution and types of the landslides in this area.

To further explore the possible causes of tunnel deformation, we analyzed the surface deformation of the study area using D-InSAR. The results show that at the time of deformation of the tunnel, there were signs of significant deformation on the ground surface. However, these deformations follow a discrete pattern that does not appear to be correlated with the landslide morphologies as obtained from the other investigations. Generally, settlement is mainly concentrated on the western side of the central gully, at the location of the L2 and L3 landslides (Fig. 13). There is a certain degree of uplift at the front edge of the L1 landslide, and landslide L5 also shows evidence of general uplift. There are signs of local downslope movements at the location of L9 landslide and this is the cause of the deformation observed along the toe of the landslide. The foregoing deformation patterns do not appear to support the possibility of a large-scale, deep-seated gravitational slope deformation. Coupled with the observed slip surface depths in the boreholes and the multiple directions of sliding movement (Fig. 10) it is therefore highly unlikely that the deformation in the tunnel can be explained by a deep-seated slip surface of a very large landslide.

A further important observation from the D-InSAR monitoring results is that in the middle and lower part of L7 landslide a linear surface feature can be observed with differential uplift and subsidence on either side. This is a typical indication of fault activity and it appears to show a fault with a NNE-SSW trend. It is reasonable to assume that this fault extends in an SSW direction to intersect with the zone where the tunnel rupture of the tunnel lining occurred and damage was observed. The movement observed for landslides L2 and L3 likely indicates the reactivation of these two secondary landslides as a result of long-term progressive erosion of the central gully, and this movement may well be a triggered by movement in the fault that cuts across the domain of landslide L3.

6 Conclusion

To examine the causes of deformation of the Zhangjiazhuang tunnel in 2016, we used a variety of methods to conduct a comprehensive investigation of the geological and geomorphic characteristics, human activity, and construction factors within the scope of the slope where the tunnel is located. Based on mapping of the engineering geomorphology of the study area, analysis of the direction of slicken-sided surface striations, and stratigraphic correlation we have reconstructed the spatial distribution and types of the landslide group in this area. From the local deformation of the factory wall in front of the landslide, the lack of deformation of the paved road, the deformation location of the tunnel, and the monitoring results of D-InSAR, we believe that deepseated gravitational deformation and the reactivation of the landslide complex are not the fundamental cause of tunnel

deformation. From the surface deformation monitoring results, the deformation of the tunnel is considered to be related to the NEE– SWW trending active fault in the area. In addition, dense networks of sinkholes developed in the study area provide conditions for rainfall and artificial irrigation infiltration, which eventually induced the reactivation of L2 and L3 landslides and formed J. Mt. Sci. (2021) 18(7): 1920-1936 1935 tensile cracks at the rear scarp of L1 landslide. However, these landslides have a slip surfaces that do not penetrate into the underlying bedrock and therefore they have no bearing on the stability of the tunnel. In the Loess Plateau of China similar geological and geomorphological settings are common, and the influence of fault activity is often ignored. Therefore, we suggest that in the construction of highway and railway tunnels and other important engineering facilities in these environments, factors such as sinkholes, faults, joints, and groundwater infiltration should be investigated in detail to enable pro-active mitigation of their possible impacts.

Acknowledgements

This work was funded by the National Key Research and Development Program of China (Grant No. 2018YFC1504704), the National Natural Science Foundation of China (Grant No. 41661144046), the Fundamental Research Funds for the Central Universities (Grant No. lzujbky-2018-k14), and the Key Research and Development Program of Gansu Province (Grant No. 18YF1WA114). We thank the Qinghai Environmental Geological Survey who provided the DEM, aerial images and drilling data, and the reviewers for their constructive comments which have substantially improved the manuscript.

References

Aimaiti Y, Yamazaki F, Liu W, et al. (2017) Monitoring of landsurface deformation in the Karamay Oilfield, Xinjiang, China, using SAR interferometry. Appl Sci 7(8): 772. https://doi.org/10.3390/app7080772

Bandini A, Berry P, Boldini D (2015) Tunnelling-induced landslides: The Val di Sambro tunnel case study. Eng Geol 196: 71-87. https://doi.org/10.1016/j.enggeo.2015.07.001

Barla G, Debernardi D, Perino A (2015) Lessons learned from deep-seated landslides activated by tunnel excavation. Geomech Tunn 8(5): 394-401. https://doi.org/10.1002/geot.201500028

Bieninwski ZT (1973) Engineering classification of jointed rock masses. Trans South Afr Institut Civil Eng 15(12): 335–343.

Casu F, Manzo M, Lanari R (2006) A quantitative assessment of the SBAS algorithm performance for surface deformation retrieval from D-InSAR data. Remote Sens Environ 102: 195- 210. https://doi.org/10.1016/j.rse.2006.01.023

Causse L, Cojean R, Fleurisson J (2015) Interaction between tunnel and unstable slope-Influence of time-dependent behavior of a tunnel excavation in a deep-seated gravitational slope deformation. Tunn Undergr Space Technol 50: 270-281. https://doi.org/10.1016/j.tust.2015.07.018

Costantini M (1998) A novel phase unwrapping method based on network programming. IEEE Trans. Geosci Romote Sens 36(3): 813-821. https://doi.org/10.1109/36.673674

Derbyshire E, Meng XM, Dijkstra TA (2000) Landslides in the thick loess terrain of North-West China. John Wiley & Sons Ltd., Chichester and New York. p 288.

Dijkstra TA, Rogers CDF, Smalley IJ, et al. (1994) The loess of north-central China: Geotechnical properties and their relation to slope stability. Eng Geol 36(3): 153-171. https://doi.org/10.1016/0013-7952(94)90001-9

Farhadian H, Aalianvari A, Karibeh H (2012) Optimization of analytical equations of groundwater seepage into tunnels: a case study of Amikabir tunnel. J Geol Soc India 80: 96-100. https://doi.org/10.1007/s12594-012-0122-z

Fernandez G, Moon J (2010) Excavation-induced hydraulic conductivity reduction around a tunnel–part 1: Guideline for estimate of ground water inflow rate. Tunn Undergr Space Technol 25(5): 567-574. https://doi.org/10.1016/j.tust.2010.03.006

Flessandro A, Prati C, Rocca F (2001) Permanent scatterers in SAR interferometry. IEEE Trans Geosci Remote Sens 39: 8- 20. https://doi.org/10.1109/36.898661

Gattinoni P, Consonni M, Francani V, et al. (2019) Tunnelling in landslide areas connected to deep seated gravitational deformations: An example in Central Alps (northern Italy). Tunn Undergr Space Technol 93: 1-17. https://doi.org/10.1016/j.tust.2019.103100

Goldstein RM, Werner CL (1998) Radar interferogram filtering for geophysical applications. Geophys Res Lett 25(21): 4035- 4038. https://doi.org/10.1029/1998GL900033

He C, Wang B (2013) Research process and development trends of highway tunnels in China. J Mod Transport 21(4): 209- 223. https://doi.org/10.1007/s40534-013-0029-4

Hoek E, Brown ET (1997). Practical estimates of rock mass strength. Int J Rock Mech Min Sci 34(8): 1365-1609. https://doi.org/10.1016/S1365-1609(97)80069-X

Hoek E, Marinos P (2000) Predicting tunnel squeezing problems in weak heterogeneous rock masses. Tunn Tunnell Int 32(11): 45-51.

Komu M, Guney U, Kilickaya TE, et al. (2020) Using 3D Numerical analysis for the assessment of tunnel–landslide relationship: Bahce–Nurdag Tunnel (South of Turkey). Geotech Geol Eng 38(4): 1237-1254. https://doi.org/10.1007/s10706-019-01084-9

Konagai K, Numada M, Zafeirako A, et al. (2005) An example of landslide-inflicted damage to tunnel in the 2004 mid-Niigata prefecture earthquake. Landslides 2: 159-163. https://doi.org/10.1007/s10346-005-0057-1

Li S, Chen Y (1999) Tunnel effect of fractal fault and transient Swave velocity rupture (TSVR) of in-plane shear fault. Earth Sci 12: 19-25. https://doi.org/10.1007/s11589-999-0003-8

Liu C, Chen P, Matsuo T, et al. (2015) Rapidly responding to landslides and debris flow events using a low-cost unmanned aerial vehicle. J App Remote Sens 9(1): 096016. https://doi.org/10.1117/1.JRS.9.096016

Ma H, Wu H (2016) Progress and expectation of research on tunnel-landslide system. Chin J Undergr Space Eng 12: 522- 530. (In Chinese)

Ma J, Tang H, Hu X, et al. (2014) Application of 3D laser scanning technology to landslide physical model test. Rock Soil Mech 35(5): 1495-1505. (In Chinese) J. Mt. Sci. (2021) 18(7): 1920-1936 1936

Ma L, Cheng L, Li M, et al. (2015) Training set size, scale, and features in Geographic Object-Based Image Analysis of very high resolution unmanned aerial vehicle imagery. J Photogramm Remote Sens 102: 14-27. https://doi.org/10.1016/j.isprsjprs.2014.12.026

Mao J, Zhou D (2002) Deformation analysis for landslidetunnel interaction. J Southwest Jiaotong Univ 37(4): 371-376. (In Chinese)

Nikadat N, Fatehi M, Abdollahipour A (2015) Numerical modelling of stress analysis around rectangular tunnels with large discontinuities (fault) by a hybridized indirect BEM. J Cent South Univ 22: 4291-4299. https://doi.org/CNKI:SUN:ZNGY.0.2015-11-024

Obradovic J (1990) Influence of Neotectonic activity on the pumped storage scheme tunnel lining behavior and failure. Thomas Telford 21: 403-413. https://doi.org/info:doi/10.1680/ps.15869

Peng JB, Fan ZJ, Wu D, et al. (2015) Heavy rainfall triggered loess–mudstone landslide and subsequent debris flow in Tianshui, China. Eng Geol 186: 79-90. https://doi.org/10.1016/j.enggeo.2014.08.015

Qi TJ, Meng XM, Qing F, et al. (2021) Distribution and characteristics of large landslides in a fault zone: A case study of the NE Qinghai-Tibet Plateau. Geomorphology 379: 107952. https://doi.org/10.1016/j.geomorph.2021.107592

Rehman MU, Zhang Y, Meng XM, et al. (2020) Analysis of landslide movements using interferometric synthetic aperture radar: a case study in Hunza-Nagar valley, Pakistan. Remote Sens 12(12): 2054. https://doi.org/10.3390/rs12122054

Singh Y, Sharma V, Pandita S, et al. (2014) Investigation of landslide at Sangaldan near tunnel-47, on Katra- Qazigund railway track, Jammu and Kashmir. J Geol Soc India 84(6): 686-692.

Song CH (2006) Tectonic uplift and Cenozoic Sedimentary evolution in the northern margin of the Tibetan Plateau. PhD thesis, Lanzhou University. p 46. (In Chinese)

Syahmi M, Aziz W, Zulkarnaini M, et al. (2011) The movement detection on the landslide surface by using Terrestrial Laser Scanning. IEEE Control & System Graduate Research Colloquium pp 174-180. https://doi.org/10.1109/ICSGRC.2011.5991851

Tang MA, Wang Y, Sun BL (2013) Application and research of geologic radar in groundwater disease of tunnel engineering inspection. Appl Mech Mater 256: 1167-1171. https://doi.org/10.1051/e3sconf/201913101063

Tian ZY, Zhang MS, Wu YZ (2019) Application of intergrated geophysical exploration in the cracks detection of the front edge in Gaojiawan. Chinese J Eng Geop 16(6): 822-828. (In Chinese)

Troncone A, Conte E, Donato A (2014) Two and threedimensional numerical analysis of the progressive failure that occurred in an excavation-induced landslide. Eng Geol 183(3): 265-275. https://doi.org/10.1016/j.enggeo.2014.08.027

Vassallo T, Mishra M, Santarsiero G, et al. (2019) Modeling of Landslide–Tunnel Interaction: the Varco d'Izzo Case Study. Geotech Geol Eng 37: 5507-5531. https://doi.org/10.1007/s10706-019-01020-x

Wang T, Li J, Chui Y, et al. (2011) Tunnel Deformation and Lining Anomalies Induced by Deep-seated Gravitational Slope Deformation. Tunn Cons 31(S1): 116-122. (In Chinese)

Wu H, Pai L (2020) Research on the Deformation Mechanisms of a Tunnel-Landslide System based on the Point Safety Factor of the Interface. E3S Web of Conferences 165: 04068. https://doi.org/10.1051/e3sconf/202016504068

Wu H, Wu D, Ma H, et al. (2012) Research on type of tunnel landslide system and tunnel deformation mode. Chin J Rock Mech Eng 31(S2): 3632-3642. (In Chinese)

Ye X, Kaufmann H, Guo X (2004) Landslide monitoring in the Three Gorges area using D-InSAR and Corner Reflectors. Photogramm Eng Remote Sens 10: 1167-1172. https://doi.org/info:doi/10.14358/PERS.70.10.1167

Zeng R, Meng X, Zhang F, et al. (2016) Characterizing hydrological processes on loess slopes using electrical resistivity tomography – A case study of the Heifangtai Terrace, Northwest China. J Hydrol 541: 742-753. https://doi.org/10.1016/j.jhydrol.2016.07.033

Zhang M, Liu J (2010) Controlling factors of loess landslides in western China. Environ Earth Sci 59: 1671-1680. https://doi.org/10.1007/s12665-009-0149-7

Zhang J, Wang YN, Zhang BH, et al. (2016) Tectonics of the Xining Basin in NW China and its implications for the evolution of the NE Qinghai-Tibetan Plateau. Basin Res 28(2): 159-182. https://doi.org/10.1111/bre.12104

Zhang Y, Lan H, Zhang Y, et al. (2013) Nonlinear dynamic failure process of tunnel-fault system in response to strong seismic event. J Asian Earth Sci 64: 125-135. https://doi.org/10.1016/j.jseaes.2012.12.006

Zhang Y, Yang J, Yang F (2015) Field investigation and numerical analysis of landslide induced by tunneling. Eng Fail Anal 47: 25-33. https://doi.org/10.1016/j.engfailanal.2014.09.011

Zhang Y, Meng XM, Chen G, et al. (2016) Detection of geohazards in the Bailong River Basin using synthetic aperture radar interferometry. Landslides 13: 1273-1284. https://doi.org/10.1007/s10346-015-0660-8

Zhang ZG, Zhao QH, Chen XU, et al. (2017) Interaction analyses between tunnel and landslide in mountain area. J Mt Sci 14(6): 1124-1139. https://doi.org/10.1007/s11629-016-3999-y

Zhou SH, Tian ZY, Di HG, et al. (2020) Investigation of a loessmudstone landslide and the induced structural damage in a high-speed railway tunnel. Bull Eng Geol Environ 79: 2201- 2212. https://doi.org/10.1007/s10064-019-01711-y

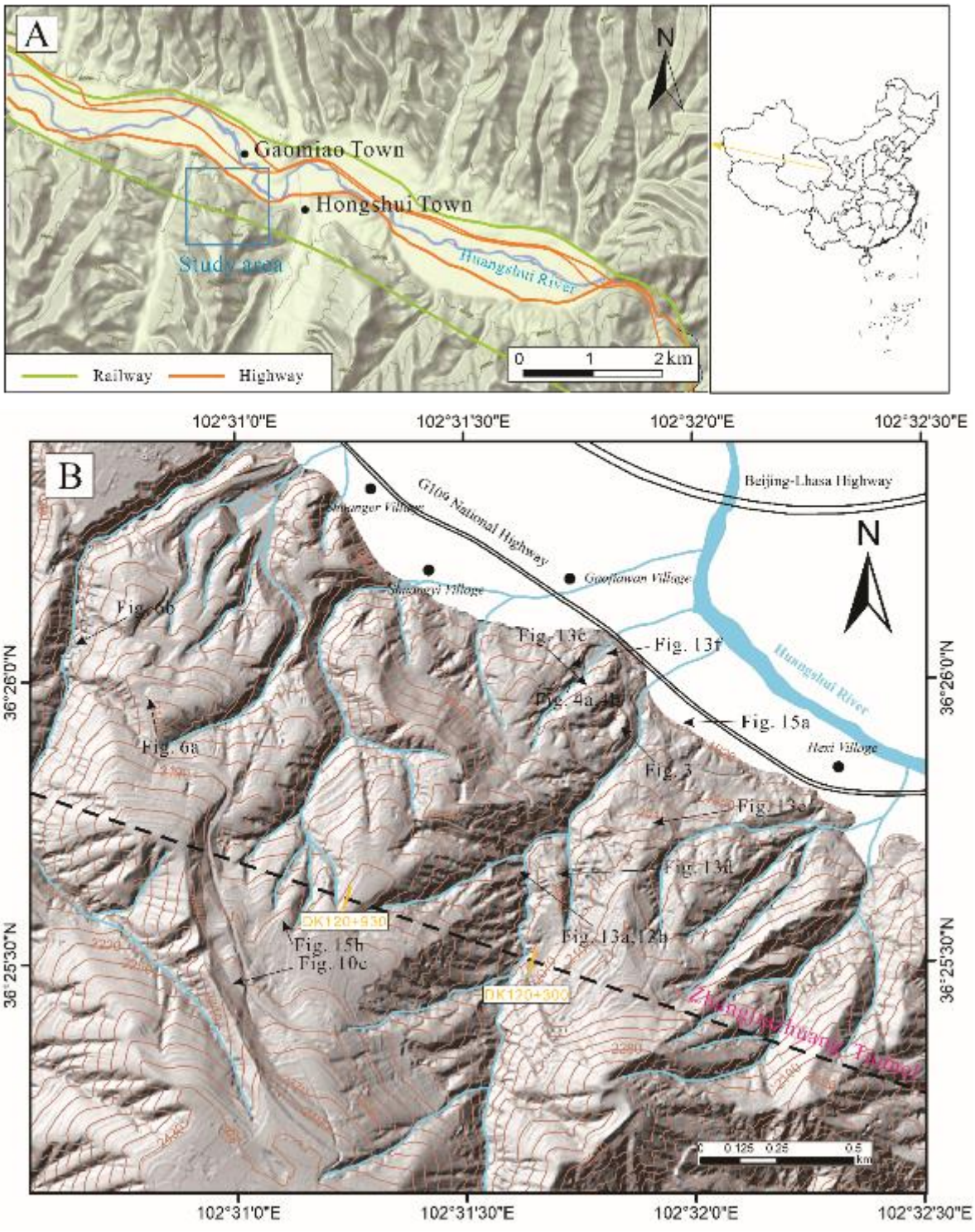

Figure 1 Location and terrain of the study area: A Location of the study area; B Digital terrain model of the study area and the location of the Zhangjiazhuang tunnel. The location of the photos used in this paper is shown in the figure.

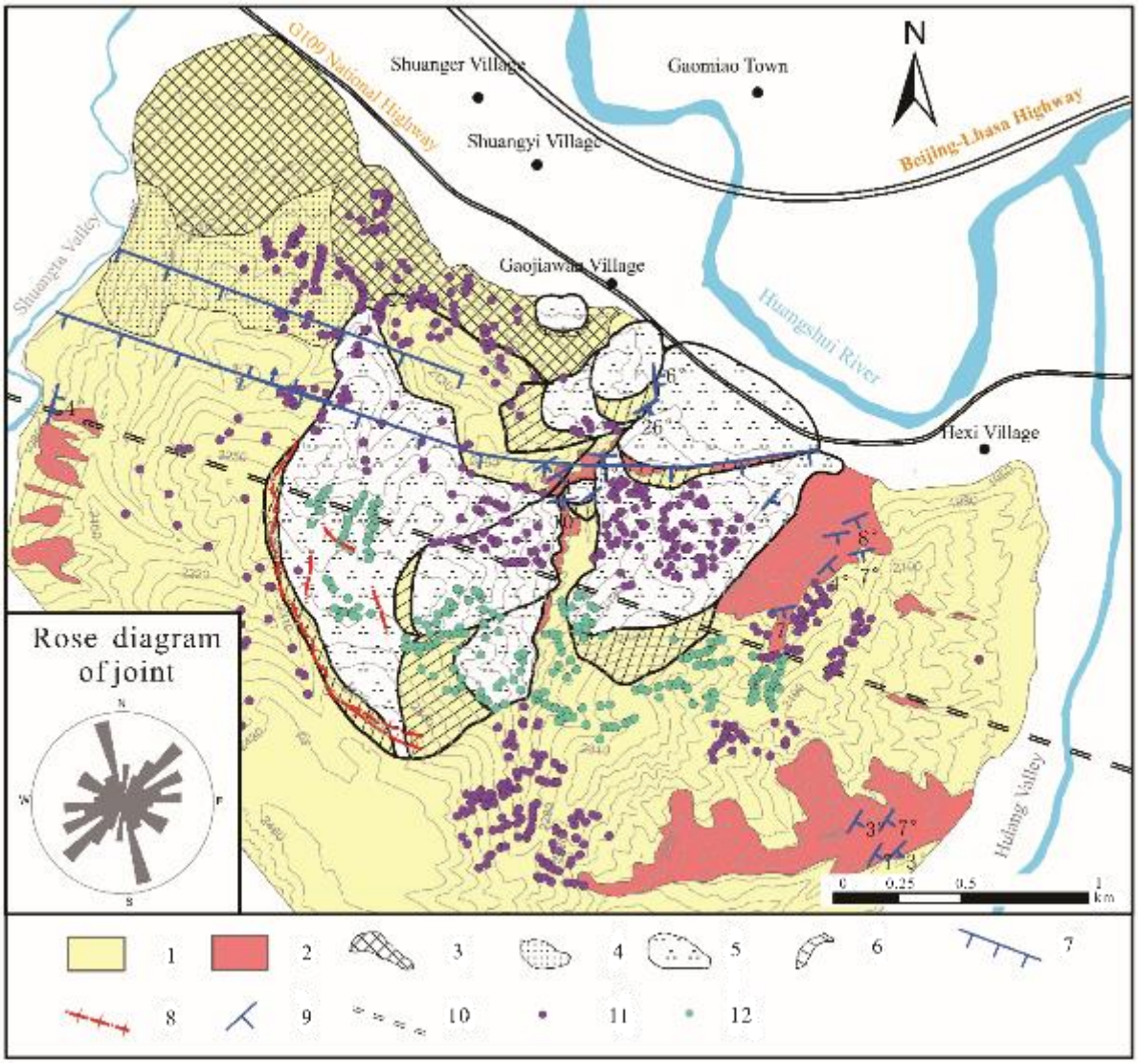

Figure 2 Engineering geomorphological map of the study area. 1) Quaternary loess; 2) mudstone; 3) 4th terrace of the Huangshui River; 4) 5th terrace of the Huangshui River; 5) ancient landslide; 6) main scarp; 7) normal fault; 8) cracks; 9) attitude of the strata; 10) Zhangjiazhuang tunnel; 11) unsealed sinkholes; 12) sealed sinkholes.

Figure 3 Typical lithologies outcropping at the Gaojiawan landslide site. The upper part is Quaternary loess and the lower part is Paleogene mudstone.

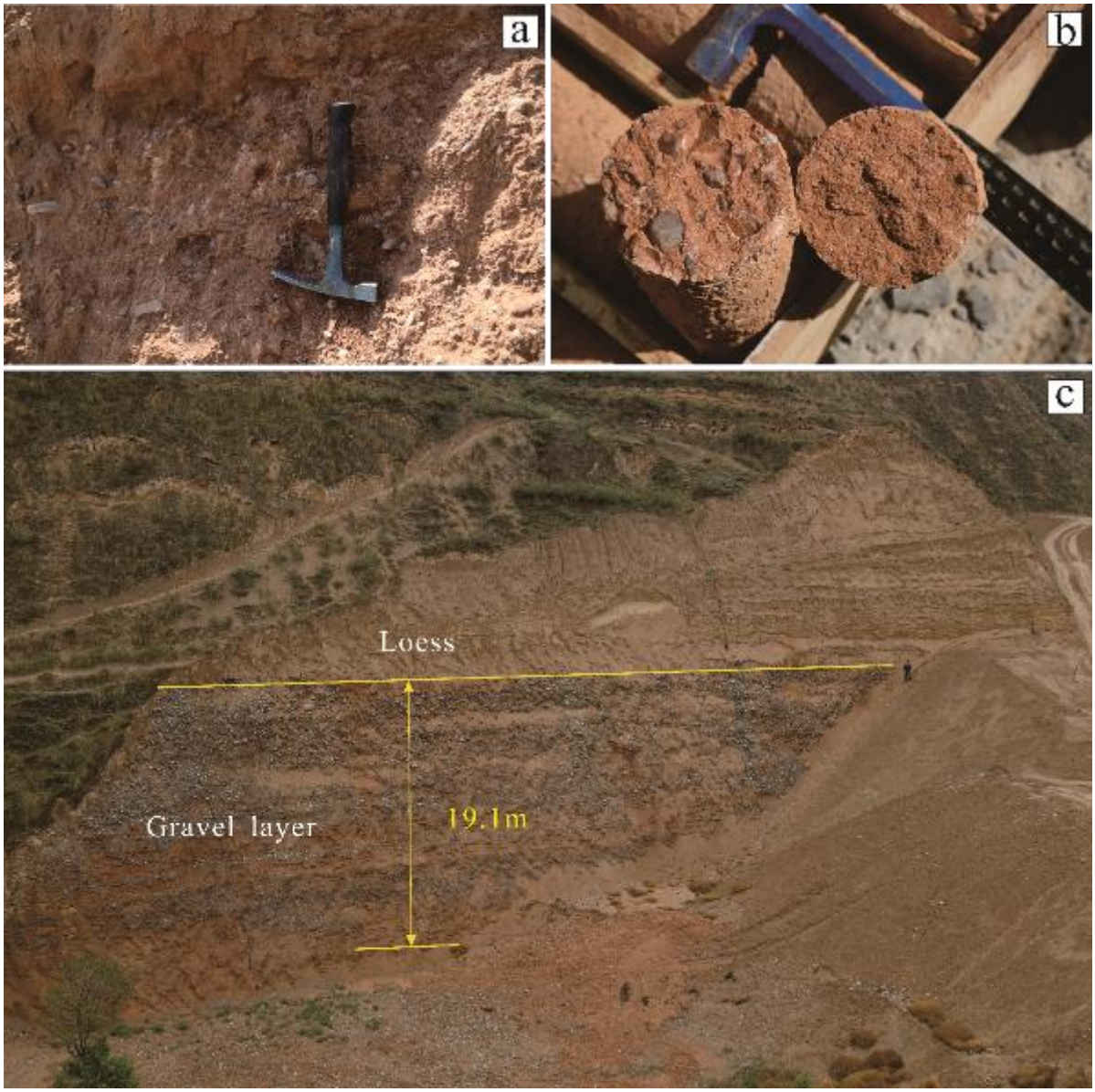

Figure 4 a. Paleocene sandstone found in the profile. b. Sandstone detected in the boreholes. c. View of the terrace.

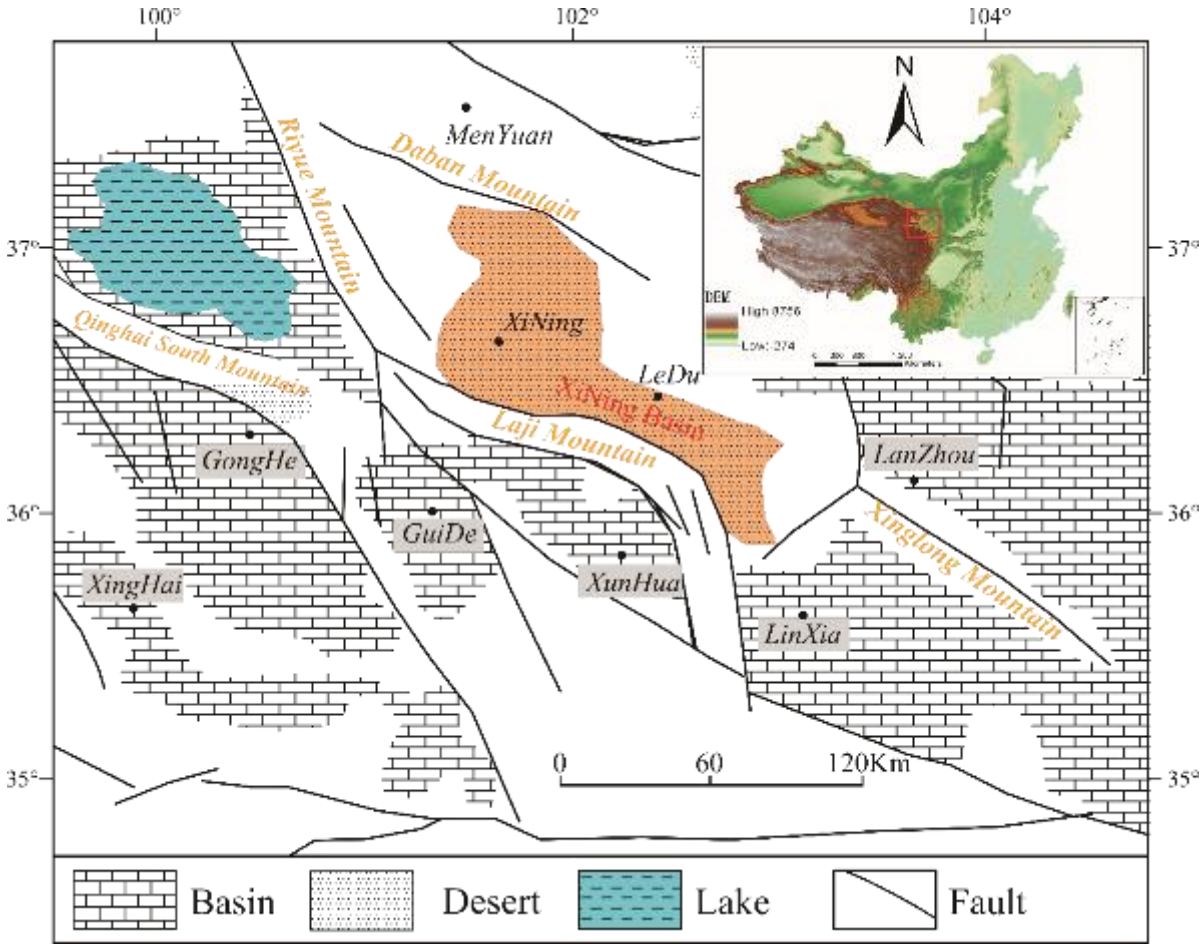

Figure 5 Structural geology map of the study area (after Song 2006).

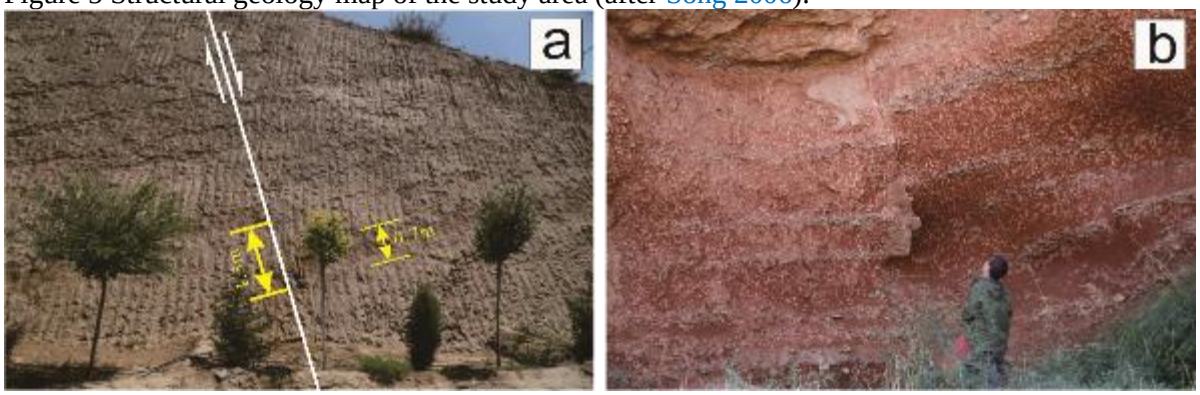

Figure 6 Tectonic structures detected in the study area. a. Paleosol layer cut by a normal fault. b. Sandstone cut by a normal fault.

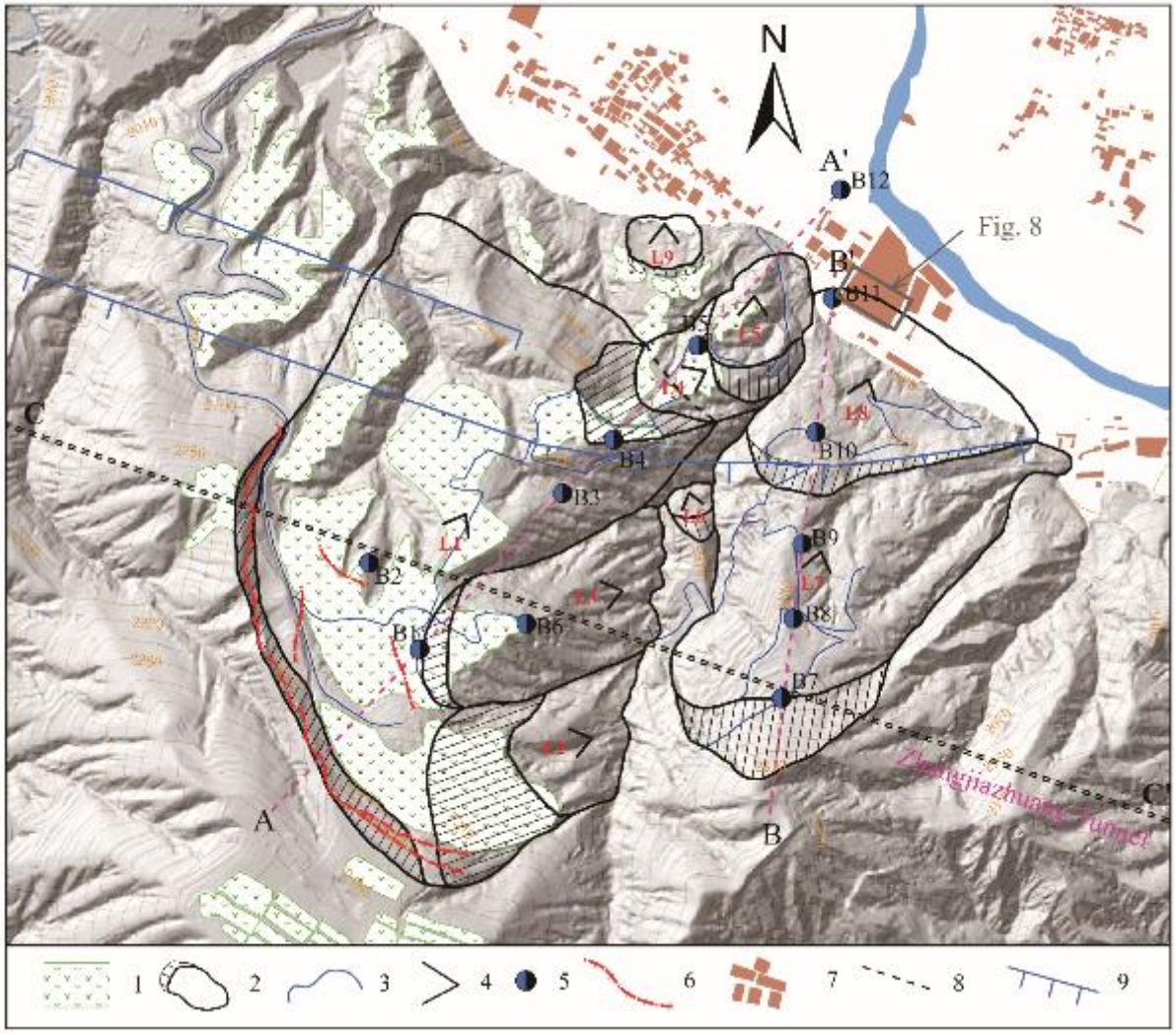

Figure 7 Landslide map produced by a field survey and photo interpretation. 1)crops; 2) landslide body and head scarp; 3) roads; 4) direction of landslide; 5) borehole; 6) cracks; 7) residential buildings; 8) inferred boundary;9) faults.

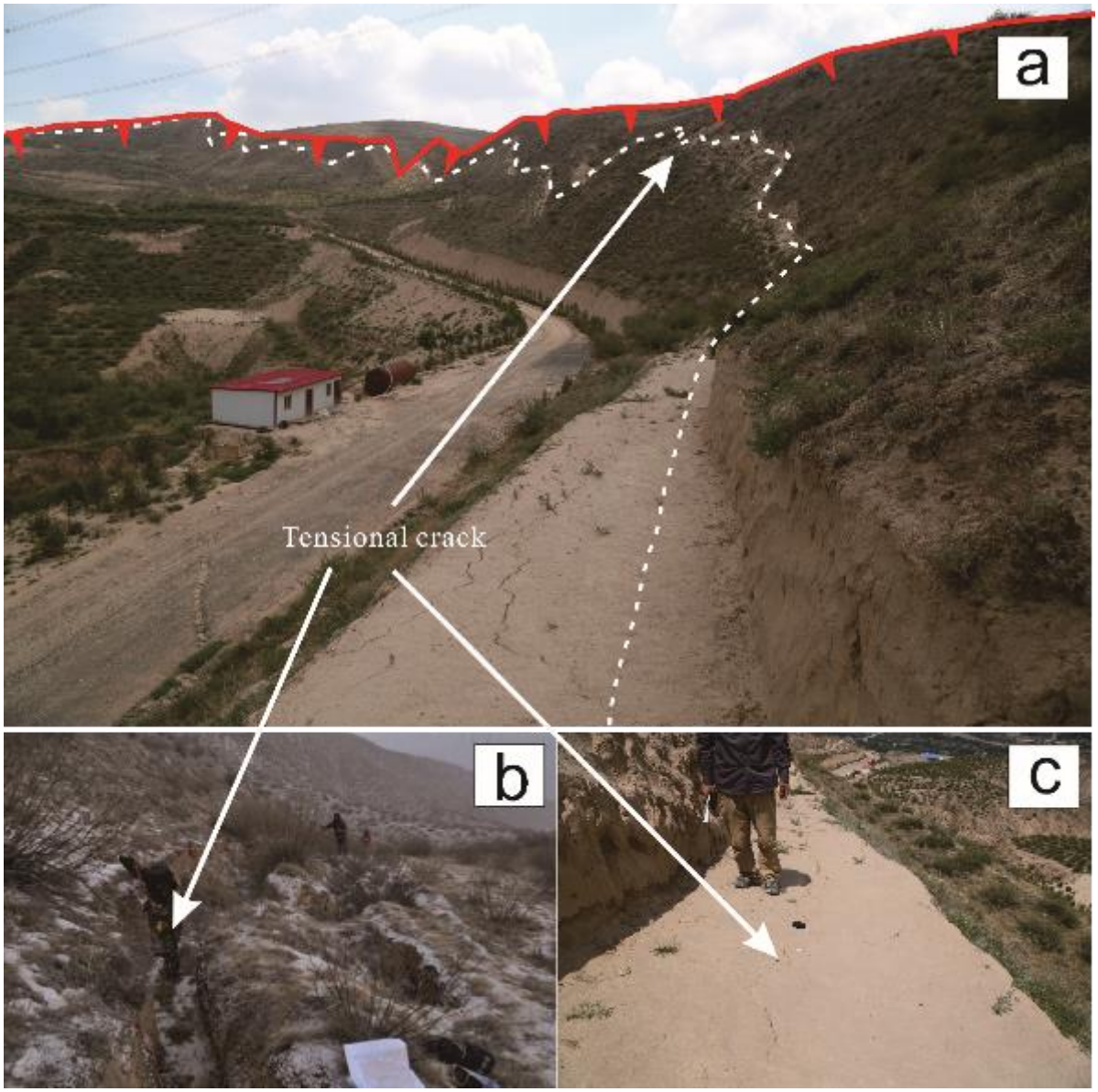

Figure 8 a and b photographs of the main scarp of the L1 and the longest fissure observed in this scarp. c new cracks appeared after tamping.

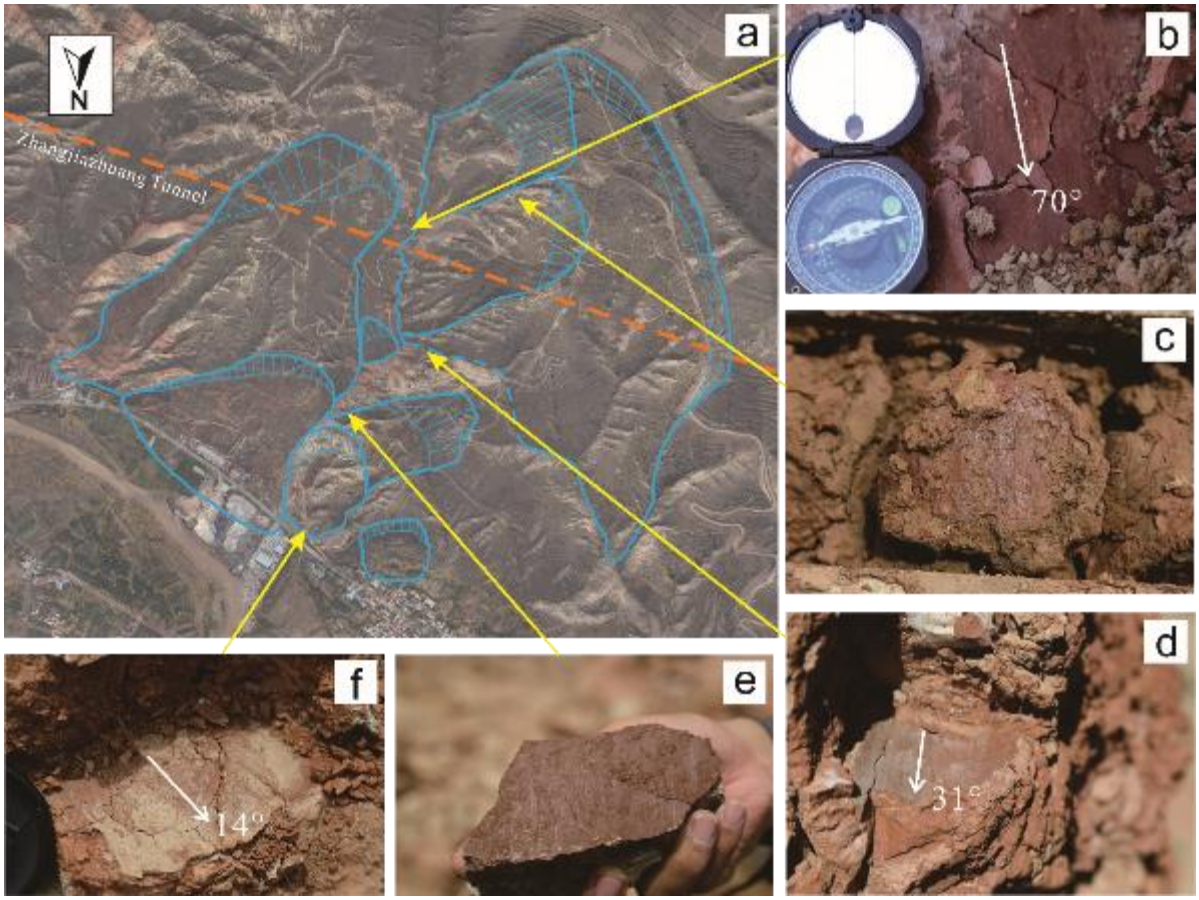

Figure 9 Examples of sliding scratches associated with the landslide group observed in the study area. a. unmanned aerial vehicle image, b. Sliding surface and direction of L2 landslide, c. The sliding surface of the L1 landslide found in the borehole, d. Sliding surface and direction of L1 landslide, e. Sliding surface of L4 landslide, f. Sliding surface of L5 landslide.

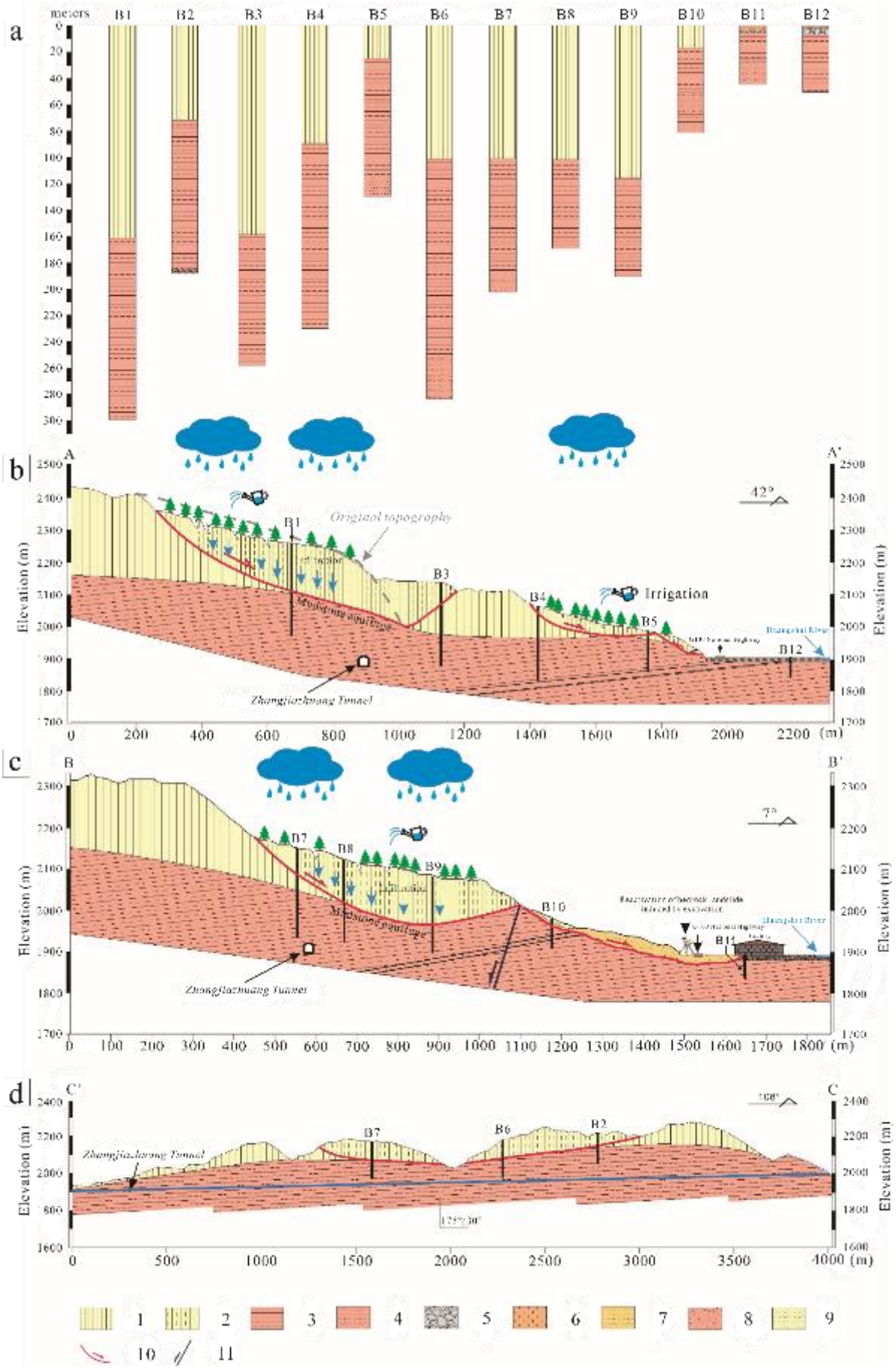
a
meters
B1
B2
B3
B4
B5
B6
B7
B8
B9
B10
B11
B12
b
A
A'
Elevation (m)
Original topography
Irrigation
Zhangjiazhuang Tunnel
Huangshui River
42°
c
B
B'
7°
Zhangjiazhuang Tunnel
d
C'
C
Zhangjiazhuang Tunnel
1
2
3
4
5
6
7
8
9
10
11

Figure 10 Longitudinal profile of the main landslides and tunnel profile. 1) loess; 2) loess landslide; 3) mudstone; 4) sandstone; 5) gravel layer; 6) bedrock landslide; 7) Quaternary sediments; 8) glutenite; 9) loess cover with bedrock landslide; 10) sliding surface; 11) fault. a. Borehole columnar profiles, b. Landslide profile of L1, L4 and L5, c. Landslide profile of L7 and L8.

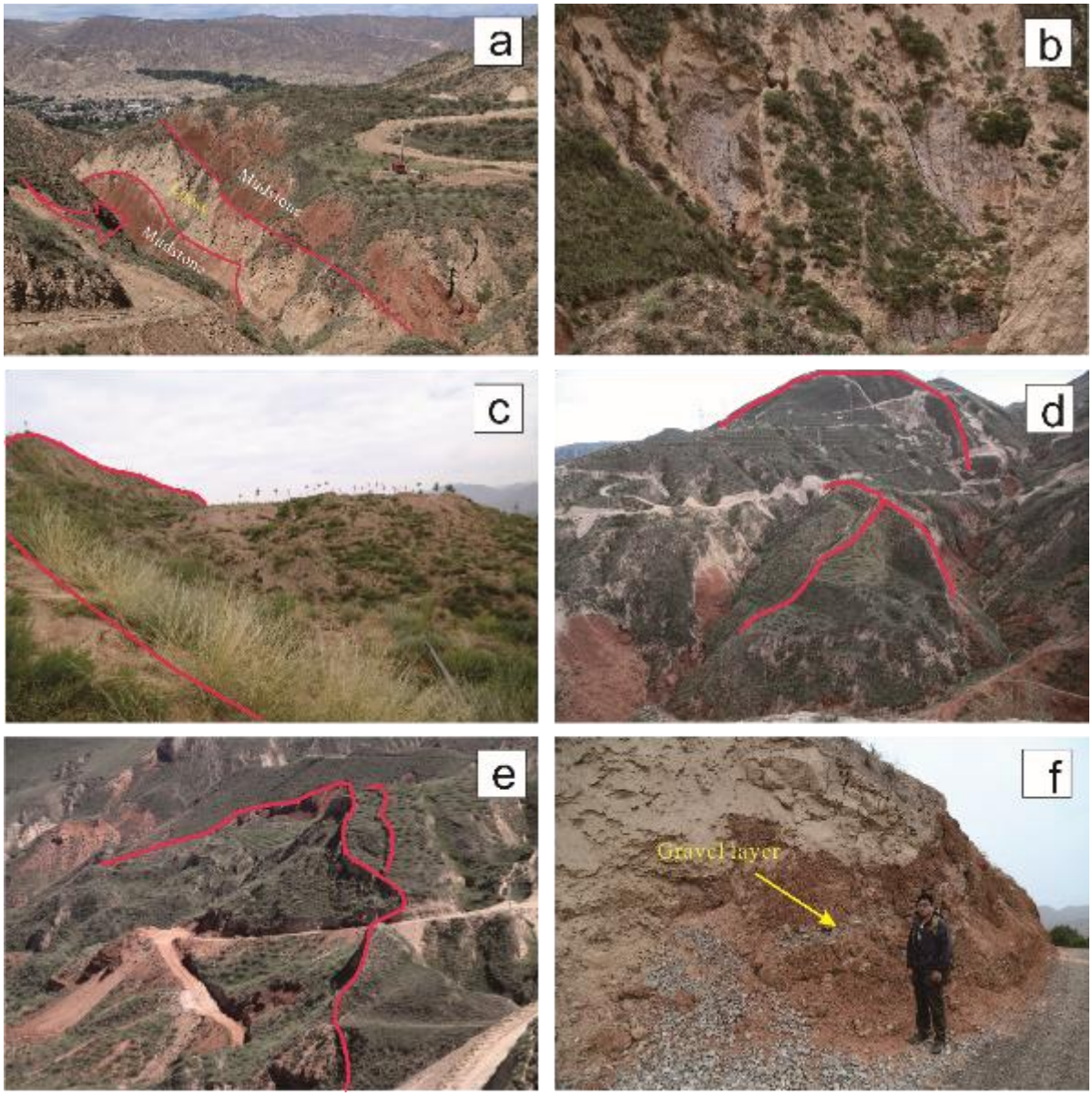

Figure 11 Photographs of the study area. a Quaternary loess sandwiched between much older mudstone. b groundwater seepage in front of L3. c main scarp of landslide L5. d main scarp of landslides L6 and L7. e main scarp and crack in landslide L8. f terrace gravel layer at the foot of landslide L5, inclined in the landslide direction

Figure 12 Example of wall deformation and extrusion at the front of the slope. a Walls of the factory located in the front of the bedrock landslide. b Arching of the east wall. c Arching of the west wall. d Sketch map of the east wall that subjected to uneven deformation. e Sketch map of the east wall that deformed with unequal spacing.

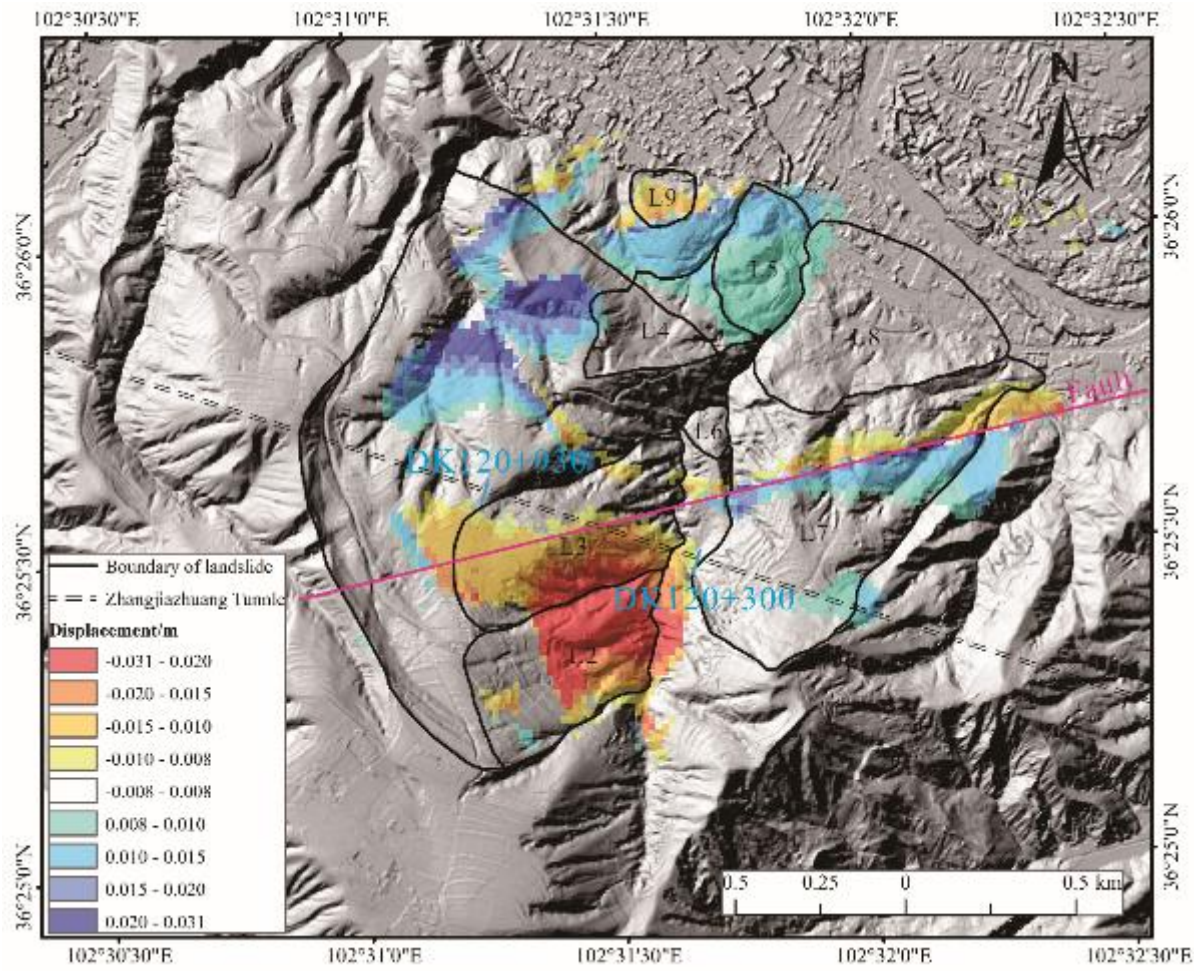

Figure 13 Surface deformation characteristics of the study area calculated by D-InSAR during 20 December 2015 and 6 February 2016.

Figure 14 Photos of the study area. a Mixed accumulation of the L8 that gravel layer of the river terrace exhibiting a reverse dip phenomenon. b Water tank used for storing water for irrigation.